Robot Localisation and Uncertainty Control with Intermittent Range-only Measurements

F. Shamsfakhr
Dep. of Industrial Engineering
University of Trento,
Trento, Italy
E–mail: farhad.shamsfakhr@unitn.it

L. Palopoli
Dep. of Information Eng. and Computer Science
University of Trento,
Trento, Italy
E–mail: luigi.palopoli@unitn.it

D. Fontanelli
Dep. of Industrial Engineering
University of Trento,
Trento, Italy
E–mail: daniele.fontanelli@unitn.it

***Abstract*—In this paper, we address the mobile robot localisation problem by combining relative measurements with intermittent measurements collected from range sensors (e.g., Ultra-Wide Band transmitters) with measurements on the relative motion of the robot. We present some basic results on the possibility of reconstructing the state using a very small number of measurements from two different anchors by setting up a system of linear equations. Next, we study how the observability of a trajectory can be quantified by the condition number of the system matrix, and hence related to the manoeuvres executed by the robot and to sampling time used to collect the measurements. As discussed in this paper, this result can be used as a basis to define control strategies aimed to maximise observability.**

I. Introduction

Wireless positioning systems such as Ultra-wide band (UWB) have increasingly gained popularity as a viable solution for localisation in indoor environments, where Global Positioning System (GPS) is not available. As an example, UWB systems based on TWR protocol which estimates the Time of Flight, (ToF) between the UWB anchors and tags can provide real-time range estimation at the level of tens of centimetres [1]. However, TWR equipped with scheduling access protocols such as TDMA, FDMA, ALOHA, etc., forces the anchors and tags to transmit a message within a time slot or a frequency band, which results in limited scalability of these systems when a large number of tags are active in the same network [2]. In addition, due to a wide range of different factors (such as limited sensing range and signal attenuation caused by interference, reflection, obstruction, etc.), the presence of reliable measurements is not *always* guaranteed [3]. What is more, massive deployment of UWB anchors is not viable in many important applications and is expensive anyway. In order to deal with this type of resource limitation, it is possible to exploit odometry, IMUs and relative measurements in between two different measurements from the anchors [4], but the real problem is that when measurements from the different anchors are collected at different times (e.g., due to their sparsity), we cannot apply standard multilateration techniques.

In this paper, we consider this exact case: a robot moves, it has a perfect knowledge of how much its has moved from the last point and in which direction, but it is able to collect one anchor measurement at a time (intermittent measurement). As discussed in this work, localisation can still be possible solving a linear system if the a sufficient number of measurements (even at different moments) from at least two different anchors. This problem can be generally be framed within the definition "state observability" (or within the related notion of "state constructibility"). However, since a non holonomic mobile robot is a non-linear system, the observability property is very much linked to the specific trajectory followed by the system rather than to the system itself. This brings us to the problem of which manoeuvres generate trajectories that are particularly easy to reconstruct. Since our approach hinges on the solution of a system of linear equations, we can establish a clear relation between observability and condition number of the system matrix. This metric is closely related to the uncertainty of the state reconstruction, and, as shown in the paper can be expressed in terms of the sequence of input applied to the system (i.e., of the trajectory followed), and of the sampling time used to collect the measurements. This technique paves the way for using the condition number as a means to generate trajectories that optimise the reconstruction uncertainty.

II. Models

In this section, we first present the system dynamic and the measurement model used for a mobile robot localisation problem. Then we will discuss the global observability analysis under a set of intermittent measurements, a condition in which either zero or one wireless ranging measurements are used at each time step for localisation.

A. Robot Model

The model of the system is a unicycle robot moving according to the following dynamics

$$\begin{bmatrix} \dot{x} \\ \dot{y} \\ \dot{\theta} \end{bmatrix} = \begin{bmatrix} v\cos\theta \\ v\sin\theta \\ \omega \end{bmatrix}, \tag{1}$$

with $\boldsymbol{s} = [x,\, y,\, \theta]^T$ as the state of the system, where x, y is the robot position and θ is the orientation of the vehicle with respect to axis X_w of the reference frame $\langle W \rangle$, where v and ω are the robot forward and angular velocities, respectively. Assuming that the velocity components are kept constant (a customary assumption) during the k-th sampling interval

$[k\delta t, (k+1)\delta t)$, with δt as the sampling period of the robot proprioceptive sensors (i.e., odometer), we can consider the following discrete–time equivalent dynamics for the robot [5]:

$$\begin{aligned} x_{k+1} &= x_k + A_k C_k, \\ y_{k+1} &= y_k + A_k S_k, \\ \theta_{k+1} &= \theta_k + \phi_k, \end{aligned}$$

where

$$\begin{cases} A_k = v_k \delta t, \\ C_k = \cos(\theta_k), & \text{if } w_k = 0 \\ S_k = \sin(\theta_k), \\ \\ A_k = 2\frac{v_k}{\omega_k}\sin(\frac{\phi_k}{2}), \\ C_k = \cos(\theta_k + \frac{\phi_k}{2}), & \text{if } w_k \neq 0 \\ S_k = \sin(\theta_k + \frac{\phi_k}{2}), \end{cases} \tag{2}$$

and where $\phi_k = \omega_k \delta t$.

B. Measurement Model

The UWB ranging is considered as the exteroceptive measurement system in this work with ToF (Time of Flight), which is regarded as the distance between the tag (mounted on the robot) and the i-th anchor, $i = 1, \ldots, n$, at time $k\delta t$, which defines the system output as

$$z_{k,i} = \gamma_{k,i}\sqrt{\big(x_k - X_i\big)^2 + \big(y_k - Y_i\big)^2}. \tag{3}$$

We assume that $\gamma_{k,i} = \{0, 1\}$, $\forall k, i$, and that $\sum_{i=1}^{n} \gamma_{k,i} \leq 1$, i.e., at each time step at most one measurement is available.

Our objective in this study is to first investigate the conditions through which it is possible for a mobile robot with dynamics (1) and with intermittent measurements (3) to reconstruct its initial state $\boldsymbol{s}_0$, assuming the knowledge of the set of intermittent ranging measurements and the sequence of the system inputs v_k and ω_k, which is an observability problem [6].

III. Observability Analysis and Metrics

In this section, we will first show how the set of intermittent ranging measurements obtained through time 0 up to K from a given number n of UWB anchor nodes can be used to reconstruct the robots' initial condition. This study can be referred to as a *global observability* problem [4]: a system is globally observable when its initial state $\boldsymbol{s}_0$ can be determined without ambiguity from a set of exteroceptive measurements. It is worth noting that, for nonlinear systems, observability is not a structural property of the system itself, but rather of its trajectories. Thus, we will particularly focus on two general types of trajectories: 1) rectilinear trajectories (obtained by $v_k \neq 0$ and $\omega_k = 0$, $\forall k$) and 2) curved trajectories (obtained by $v_k \neq 0$ and $\omega_k \neq 0$, $\forall k$). Next, we will discuss how the observability analysis can potentially yield uncertainty control using robot trajectory synthesis and/or measurements sampling time control through system observability maximisation.

A. Global observability analysis

We will start by recalling a result of [4].

Theorem 1. *Consider a robot with kinematic* (2)*, output function* (3)*, $n = 1$ anchor and with known ego-motion data. The system state is unobservable for any trajectory.*

Proof. See [4]. □

Let us now switch to a more compelling case of Theorem 1, in which we extend the result that a curved trajectory with $n = 2$ anchors is globally observable when ranging measurements are collected simultaneously, while rectilinear paths are not [4]. Indeed, we analyse the problem by adding the measurement intermittency: notice that in this case as well, the observability property depends on the specific trajectory followed (i.e., for rectilinear trajectories, the state $\boldsymbol{s}_0$ is not observable). In particular, if the robot moves along a curved trajectory and it is able to collect a sufficient number of intermittent ranging measurements, then the system state is globally observable, as reported in the next theorem.

Theorem 2. *Consider a robot with kinematic* (2)*, output function* (3)*, $n = 2$ anchors and with known ego-motion, i.e., A_k, C_k, S_k and ϕ_k in* (2) *are supposed to be known exactly. If the robot moves on a curved trajectory (i.e., $v_k \neq 0$ and $\omega_k \neq 0$ for $k = 0, \ldots, K$) and collects at least $m = 3$ ranging measurements for each of the two anchors, $\boldsymbol{s}_0$ is globally observable.*

Proof. Let us define with $\mathbf{p}_k = [x_k,\, y_k]^T$ the position of the robot, where $\mathbf{p}_0$ is of course its initial position. Moreover, assuming that the vehicle is moving on a curved trajectory, let us define the sequence of robot manoeuvres up to time $k\delta t$ as

$$\begin{aligned} f_k &= \sum_{i=0}^{k} \frac{v_i}{\omega_i}\Big(\sin\sum_{j=0}^{i}\phi_j - \sin\sum_{j=0}^{i-1}\phi_j\Big), \\ g_k &= \sum_{i=0}^{k} \frac{v_i}{\omega_i}\Big(\cos\sum_{j=0}^{i}\phi_j - \cos\sum_{j=0}^{i-1}\phi_j\Big) - \frac{v_0}{\omega_0}, \end{aligned} \tag{4}$$

which are obtained by the sequence of inputs defined in (2). Therefore, the sequence of positions $\mathbf{p}_k$ can be given by the following linear relations

$$\begin{aligned} \mathbf{p}_1 &= \mathbf{p}_0 + \begin{bmatrix} f_0 & g_0 \\ -g_0 & f_0 \end{bmatrix}\begin{bmatrix} c_0 \\ s_0 \end{bmatrix}, \\ \mathbf{p}_2 &= \mathbf{p}_0 + \begin{bmatrix} f_1 & g_1 \\ -g_1 & f_1 \end{bmatrix}\begin{bmatrix} c_0 \\ s_0 \end{bmatrix}, \\ &\vdots \\ \mathbf{p}_{K+1} &= \mathbf{p}_0 + \begin{bmatrix} f_K & g_K \\ -g_K & f_K \end{bmatrix}\begin{bmatrix} c_0 \\ s_0 \end{bmatrix}, \end{aligned} \tag{5}$$

where $c_0 = \cos(\theta_0)$ and $s_0 = \sin(\theta_0)$.

Consider two anchors located in X_1, Y_1 and X_2, Y_2, respectively. Now, let us assume that six measurements form the two anchors at arbitrarily different time steps $\mathcal{K} = \{k_1, \ldots, k_6\}$ are collected, i.e., the set of measurements (3)

is $\{z_{k_1,1},\, z_{k_2,1},\, z_{k_3,1},\, z_{k_4,2},\, z_{k_5,2},\, z_{k_6,2}\}$, that is three from each anchor at arbitrary time steps.

By defining the following quantities $F = [f_{k_1-1},\, \ldots,\, f_{k_6-1}]$, $G = [g_{k_1-1},\, \ldots,\, g_{k_6-1}]$, $\delta z_{i,j}^{(m)} = z_{k_i,m}^2 - z_{k_j,m}^2$, $\delta f_{i,j} = f_{k_i-1} - f_{k_j-1}$, $\delta g_{i,j} = g_{k_i-1} - g_{k_j-1}$ (where f_k and g_k are given in (4)), $\alpha_i^{(1)} = f_{k_i-1}X_1 - g_{k_i-1}Y_1$, $\beta_i^{(1)} = g_{k_i-1}X_1 + f_{k_i-1}Y_1$, $\alpha_{i,j}^{(2)} = \delta f_{i,j}X_2 - \delta g_{i,j}Y_2$ and $\beta_{i,j}^{(2)} = \delta g_{i,j}X_2 + \delta f_{i,j}Y_2$, we can define the following vector of measurements

$$\boldsymbol{h} = \frac{1}{2}\begin{bmatrix} \delta z_{2,1}^{(1)} - f_{k_2-1}^2 - g_{k_2-1}^2 \\ \delta z_{3,1}^{(1)} - f_{k_3-1}^2 - g_{k_3-1}^2 \\ \delta z_{5,4}^{(2)} + f_{k_4-1}^2 + g_{k_4-1}^2 - f_{k_5-1}^2 - g_{k_5-1}^2 \\ \delta z_{6,4}^{(2)} + f_{k_4-1}^2 + g_{k_4-1}^2 - f_{k_6-1}^2 - g_{k_5-1}^2 \end{bmatrix}, \tag{6}$$

and the following motion matrix

$$\mathbf{M} = \begin{bmatrix} g_{k_2-1} & f_{k_2-1} & -\beta_1^{(1)} & -\alpha_1^{(1)} \\ g_{k_3-1} & f_{k_3-1} & -\beta_2^{(1)} & -\alpha_2^{(1)} \\ -\delta g_{3,4} & -\delta f_{3,4} & \beta_{3,4}^{(2)} & \alpha_{3,4}^{(2)} \\ -\delta g_{3,5} & -\delta f_{3,5} & \beta_{3,5}^{(2)} & \alpha_{3,5}^{(2)} \end{bmatrix}. \tag{7}$$

By defining $q = [s_0, -c_0]\mathbf{p}_0$ and $b = [c_0, s_0]\mathbf{p}_0$, we have

$$\mathbf{d} = \begin{bmatrix} q \\ b \\ c_0 \\ s_0 \end{bmatrix} \Rightarrow \mathbf{h} = \mathbf{M}\mathbf{d},$$

yielding the following Least Squares (LS) solution

$$\hat{\mathbf{d}} = (\mathbf{M}^T\mathbf{M})^{-1}\mathbf{M}^T\boldsymbol{h}. \tag{8}$$

Therefore the state estimate $\hat{\boldsymbol{s}}_0$ can be derived as

$$\hat{x}_0 = \frac{\hat{b}\hat{c}_0 + \hat{q}\hat{s}_0}{\hat{c}_0^2 + \hat{s}_0^2}, \quad \hat{y}_0 = -\frac{\hat{q}\hat{c}_0 - \hat{b}\hat{s}_0}{\hat{c}_0^2 + \hat{s}_0^2}, \quad \hat{\theta}_0 = \arctan\left(\frac{\hat{s}_0}{\hat{c}_0}\right), \tag{9}$$

where the normalisation $\hat{c}_0^2 + \hat{s}_0^2$ is introduced to compensate for residual uncertainties on the solution $\hat{\mathbf{d}}$ in (8) (more on this point in Section IV).

To conclude the discussion, when the vehicle is following a rectilinear path (i.e., $v_k \neq 0$ and $\omega_k = 0$, $\forall k$), the matrices in (5) boil down to $v_k\delta t I_2$ and, hence, there is no solution to (8) for $m = 2$. □

It is worthwhile to note that, for rectilinear trajectories, a number of $n > 2$ non collinear anchors are needed to have a solution to (5), thus yielding the same result of [4].

B. Observability metric: the Condition number

The closeness to singularity for the estimation error covariance matrix of $\hat{\boldsymbol{s}}_0$ in (8) determines the degree of observability of the system state [7]. However, if the residual of the linear solution (8) is small or moderate, the sensitivity of the least square problem to the perturbations in the coefficient matrix $\mathbf{M}$ is quickly dominated by the condition number $\kappa(\mathbf{M})$ [8]. The importance of condition number as an observability metric is three-fold. First, it allows us to get insights into the degree of observability of the system and thereby the initial state estimation uncertainty. Second, the structure of the two stochastic components of (8), i.e., $\mathbf{M}$ and $\boldsymbol{h}$, makes the derivation of a closed form covariance rather involved and challenging. Third, due to the high nonlinearity of the system equations and the high condition number, the computation of the resulting statistical moments based on the first or second order Taylor expansion can be highly inaccurate even in the presence of small measurement uncertainties. Therefore, we first derive an explicit form of the condition number of $\mathbf{M}$, which, for a square non-singular matrix, is defined as $\kappa(\mathbf{M}) = \|\mathbf{M}\|\|\mathbf{M}^{-1}\|$, where $\|.\|$ represents the Frobenius matrix norm induced by the (vector) Euclidean norm and given by the ratio between the maximum and minimum eigenvalue of $\mathbf{M}$. For a rectangular matrix $\mathbf{M}$, $\kappa(\mathbf{M}) = \|\mathbf{M}\|\|\mathbf{M}^+\|$, where $\mathbf{M}^+$ is the pseudo inverse of the matrix $\mathbf{M}$. Hence, given (8) for the two anchors case, we have

$$\begin{aligned} \kappa(\mathbf{M}) =& \|\mathbf{M}\|\|\mathbf{M}^{-1}\| \\ =& \sqrt{\frac{(L_1u_1 + L_2u_2)(L_2u_1u_3^2 + L_1u_2u_4^2)}{u_3^2u_4^2D}} \end{aligned} \tag{10}$$

where

$$\begin{aligned} L_1 =& 1 + X_1^2 + Y_1^2, \\ L_2 =& 1 + X_2^2 + Y_2^2, \\ D =& (X_1 - X_2)^2 + (Y_1 - Y_2)^2, \\ u_1 =& f_{k_2-1}^2 + f_{k_3-1}^2 + g_{k_2-1}^2 + g_{k_3-1}^2, \\ u_2 =& 2f_{k_4-1}^2 - 2f_{k_4-1}(f_{k_5-1} + f_{k_6-1}) + f_{k_5-1}^2 + f_{k_6-1}^2 + \\ & + 2g_{k_4-1}^2 - 2g_{k_4-1}(g_{k_5-1} + g_{k_6-1}) + g_{k_5-1}^2 + g_{k_6-1}^2, \\ u_3 =& -f_{k_4-1}g_{k_5-1} + f_{k_4-1}g_{k_6-1} + f_{k_5-1}g_{k_4-1} + \\ & + f_{k_6-1}g_{k_5-1} - f_{k_5-1}g_{k_6-1} - f_{k_6-1}g_{k_4-1}, \\ u_4 =& f_{k_3-1}g_{k_2-1} - f_{k_2-1}g_{k_3-1}. \end{aligned}$$

As it can be readily observed, for each anchor configuration, the system inputs ω_k and v_k, the sampling time δt and the measurement times $\mathcal{K}$ have a direct impact on the condition number of the LS solution. This fact shows that the analysis of the condition number can be employed to control the initial state reconstruction uncertainty by a suitable choice of the vehicle inputs and of the measurement sampling instants. In the next section, we will provide the empirical evidence of the solution (10) and will show how it can accurately model the system uncertainty.

IV. Results and Discussions

To substantiate with empirical evidence the analysis carried out in this paper, we assume a sampling time $\delta t = 100$ ms and a time horizon of $K = 60$ time steps, i.e., $k = 0, \ldots, K$. The unicycle moves with a constant linear velocity $v_k = 1$ m/s, $\forall k$. The vehicle is assumed to move on a curved trajectory (indeed, for rectilinear trajectories no solution exists, as stated in Theorem 2), with angular velocity $\omega_k = l0.1$ rad/s. Six intermittent ranging measurements are collected at times $\mathcal{K} = [0,\, 11,\, 23,\, 35,\, 47,\, 59]$. We assume two anchors deployed

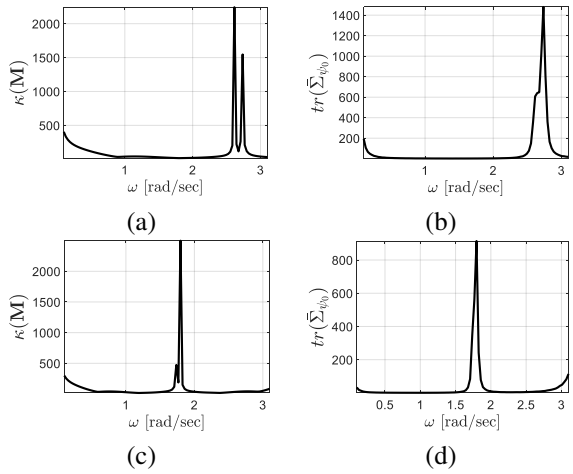

Fig. 1. Condition number (a,c) and corresponding state estimation error (b,d) of the LS solution versus 200 different angular velocities ranging from 0.1 rad/s to 3.1 rad/s. Two different sets of ranging measurements are considered, which are chosen equally spaced in the interval $k = 0, \ldots, 60$ (a,b) and $k = 0, \ldots, 90$ (c,d).

randomly in the environment, while three measurements are collected from each anchor. The analysis of the explicit form of the condition number derived in (10) is reported in Figure 1-a versus the angular velocity, computed along 200 sampling points with $l \in [1, 31]$. To expose the influence of the measurement sampling instants, Figure 1-c reports the results for $K = 90$ time steps, with ranging measurements sampling instants given by $\mathcal{K} = [0,\ 17,\ 35,\ 53,\ 71,\ 89]$. Next for the analysis of the initial state estimation sample covariance, a Monte Carlo (MC) test with 5000 iterations was carried out for each selected value of the angular velocity ω_k, where i.i.d. zero-mean Gaussian uncertainties were applied on both the system inputs and ranging measurements. The standard deviation of the additive uncertainty for the linear and angular velocities were $\sigma_v = 0.1$ m/s and $\sigma_\omega = 0.05$ rad/s, respectively, while for the ranging measurements $\sigma_z = 0.05$ m, which superimpose a fairly moderate noisy condition to the system.

Here, two important points should be emphasised. First, the condition number is independent from the initial pose of the robot. In other words, for any random initial pose, the condition number in Figure 1 is exactly the same, whereas this is not necessarily true for the initial state sample covariance. However, the different pose in the same environment will majorly change the magnitude of the error in the graphs of Figure 1, while the shape of the uncertainty remains qualitatively the same for any pose in the same environment. This fact will be further empirically proved through the next set of simulations. Second, the MC test is only used for the computation of the covariance matrix and not for the condition number. As can be seen from the Figure 1, the trace of the state estimation error covariance (obtained by MC for a fixed initial pose) and the condition number are quite similar, indicating that the condition number of the LS solution can effectively be used as a metric for the state observability degree.

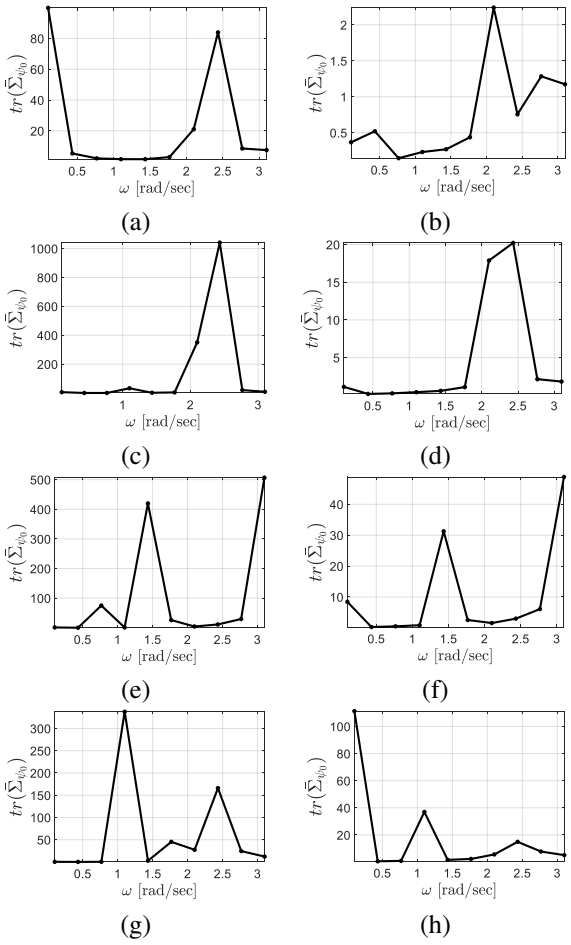

Fig. 2. State estimation error variance of LS (a,c,e,g) and NLLS (b,d,f,h) with different angular velocities with the same initial configuration and the same number of time steps (i.e., $K = 70$). The robot internal measurement sampling time for the first case (a, b) is $\delta t = 0.1$ ms, for the second case (c, d) is $\delta t = 0.2$ ms, for the third case (e, f) is $\delta t = 0.3$ ms and for the fourth case (g, h) is $\delta t = 0.4$ ms.

In the second set of simulations, the comparison between (8) and a Nonlinear Least Squares (NLLS) solution was carried out. In addition, in this analysis the impact of robot internal sampling frequency δt on the initial state estimation uncertainty was investigated. The NLLS solution is computed from an initial state $\hat{\boldsymbol{s}}_0$. As a consequence, the first step of the solution identifies the correction $\Delta_{\boldsymbol{s}_0}$ as

$$\Delta_{\mathbb{S}_0} = (\mathbf{J}^T\mathbf{J})^{-1}\mathbf{J}^T(Z - \hat{Z}). \tag{11}$$

which is derived by using the first order Taylor approximation, with the matrix $\mathbf{J} = [d_{z_0}^T, d_{z_1}^T \ldots, d_{z_5}^T]^T$, as the Jacobian of the measurement function (3), and $d_{z_0}^T$ as the vector of partial derivatives of the measurement function with respect to the parameters, i.e, $[x_0,\ y_0,\ s_0,\ c_0]$. Notice that Z and $\hat{Z}$ are the vector of the actual and estimated ranging measurements, respectively. Following the approach in [9], we finally find the initial correction $\Delta_{\boldsymbol{s}_0}$ that iteratively refine the initial state estimate as follows

$$\hat{\boldsymbol{s}}_0^{(i+1)} = \hat{\boldsymbol{s}}_0^{(i)} + \Delta_{\boldsymbol{s}_0},$$

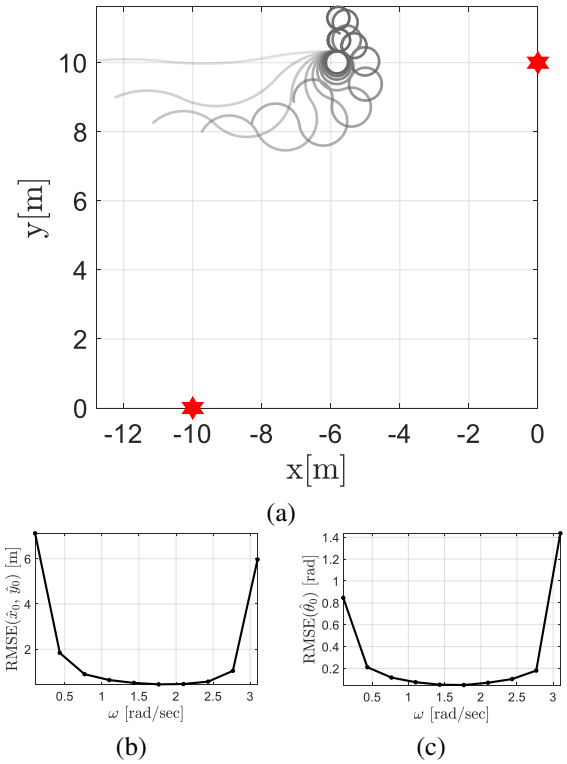

Fig. 3. Performance analysis of the proposed linear solution in reconstructing the initial position of a robot (i.e. $x_0 = -5.8$ m, $y_0 = 10.3$ m and $\theta_0 = -3.1$ rad) with 10 different curved trajectories generated with in the set (12). The RMSE plots related to the (b) initial position $\mathbf{p}_0$ and (c) orientation θ_0 estimate are reported as a function of the angular velocity ω_k. The impact of the different ω_k from 0.1 rad/s to 3.1 rad/s on the generated trajectories are qualitatively illustrated in (a) by changing the trajectory colour from light grey to dark grey, respectively.

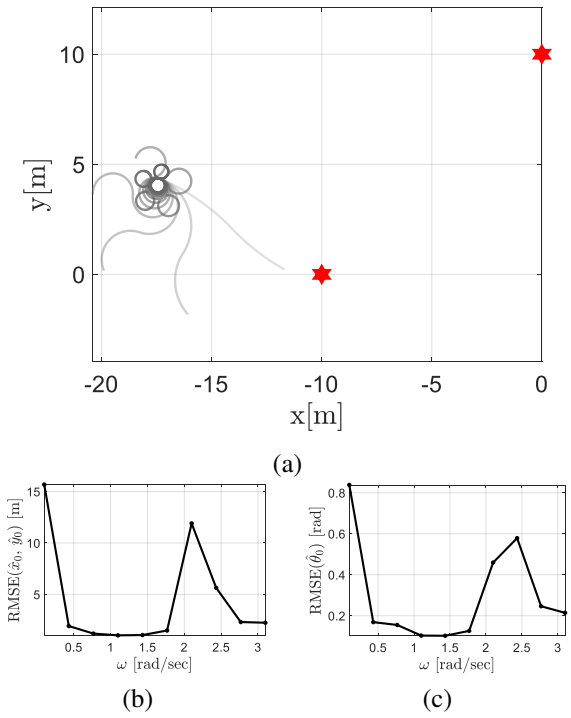

Fig. 4. Performance analysis of the proposed linear solution in reconstructing the initial position of a robot (i.e. $x_0 = -17.3$ m, $y_0 = 4.3$ m and $\theta_0 = -0.4$ rad) with 10 different curved trajectories generated with in the set (12). The RMSE plots related to the (b) initial position $\mathbf{p}_0$ and (c) orientation θ_0 estimate are reported as a function of the angular velocity ω_k. The impact of the different ω_k from 0.1 rad/s to 3.1 rad/s on the generated trajectories are qualitatively illustrated in (a) by changing the trajectory colour from light grey to dark grey, respectively.

where the index i identifies the number of iterations of the NLLS. The final solution thus obtained minimises the difference between the actual set of measurements Z and the estimated measurements $\hat{Z}$ obtained by (5).

At the end of the iterations, the vector $\hat{\mathbf{s}}_0^{(i)}$, is trivially converted to $\mathbf{d}^{(NLLS)} = [q,\, b,\, s_0,\, c_0]$, and the initial state estimation covariance is calculated in an MC fashion with 10000 iterations for both approaches. In order to make this analysis sensible, we kept the initial state for both solutions the same. For the sake of this analysis, the initial guess at the start of the NLLS algorithm $\hat{\mathbf{s}}_0$ was defined as the true initial state superimposed by an i.i.d. zero-mean Gaussian noise with standard deviation as $\sigma_{x_0} = 0.5$ m, $\sigma_{y_0} = 0.5$ m and $\sigma_{\theta_0} = 0.3$ rad for each MC trial. The results of the comparison are reported in Figure 2. In all the reported simulations, the robot moves for $K = 70$ time steps and collects the measurements at times $\mathcal{I} = [0,\, 13,\, 27,\, 41,\, 55,\, 69]$. The test was repeated four times with four different robot internal measurement sampling time δt, as shown in the Figure 2: the LS and NLLS solutions are quite similar which indicates the reliability of the LS solution.

Finally in the last scenario, the performance of the solution (8) with six intermittent measurements has been investigated in two different configurations. In both cases, the robot generates a curved trajectory with 10 different values of constant ω_k ranging from 0.1 rad/s to 3.1 rad/s with constant forward velocity of $v_k = 1$ m/s, while an i.i.d. zero-mean Gaussian noise were applied on both the system inputs and ranging measurements with standard deviations as $\sigma_v = 0.1$ m/s, $\sigma_w = 0.05$ rad/s and $\sigma_z = 0.05$ m. Figure 3, demonstrates the first scenario in which the robot generates 10 different curved trajectories with the following angular motion pattern

$$\Omega_1 = [\mathbb{1}_{1:20} \times \omega_k, \quad -\mathbb{1}_{1:30} \times \omega_k, \quad \mathbb{1}_{1:20} \times \omega_k], \qquad (12)$$

i.e., with clockwise and counterclockwise rotations. In particular, $\mathbb{1}_{1:j}$ is a row vector with all ones with length j elements. The toy trajectory obtained is depicted in Figure 3-a. The Root Mean Squared Error (RMSE) plots related to the initial position and orientation estimations which are computed through MC simulations with 10000 trials are depicted in Figure 3-b and Figure 3-c. Figure 4, illustrates the second simulation scenario in which the robot moves with the following angular velocity

$$\Omega_2 = [-\mathbb{1}_{1:40} \times \omega_k, \quad \mathbb{1}_{1:20} \times \omega_k, \quad \mathbb{1}_{1:10} \times \omega_k]. \qquad (13)$$

The RMSE plots related to the initial position and orientation

TABLE I
MAXIMUM AND MINIMUM RMSE WITH DIFFERENT VALUES OF THE UNCERTAINTIES WHEN THE NORMALISATION (9) IS APPLIED OR NOT.

Uncertainty			RMSE$_{x,\,y}$[m] (9)		RMSE$_{x,\,y}$[m] (14)	
σ_v	σ_ω	σ_z	min	max	min	max
0.01	0.01	0.01	0.08	2.63	0.15	5.26
0.02	0.02	0.02	0.16	4.55	0.31	$17 \cdot 10^3$
0.04	0.03	0.03	0.25	5.22	0.49	$1.14 \cdot 10^5$
0.08	0.04	0.04	0.35	5.94	0.69	$2.72 \cdot 10^5$
0.1	0.05	0.05	0.44	7.19	0.87	$5.9 \cdot 10^5$

estimations for the second scenario are depicted in Figure 4-b and Figure 4-c. As can be seen, in both cases, the RMSE depends on the chosen trajectory. In particular, it becomes evident how the chosen trajectory, the angular velocity value ω_k, do have an impact on the achievable RMSE.

Finally, Table I, shows the numerical inconsistency of the solution (14) in the presence of different levels of uncertainties. In particular the table reports the numerical results of the first scenario (Figure3) in terms of minimum and maximum RMSE along x and y, when the normalisation (9) is applied and when it is not applied

$$\hat{x}_0 = \hat{b}\hat{c}_0 + \hat{q}\hat{s}_0, \quad \hat{y}_0 = \hat{b}\hat{s}_0 - \hat{q}\hat{c}_0, \tag{14}$$

thus proving the benefit of the normalisation factor.

V. CONCLUSIONS

In this paper we have presented some observability results for a mobile robot moving across a space instrumented with a sparse infrastructure of range sensors. We have discussed conditions to reconstruct the state collecting measurements from two anchors. We have also studied how, in these conditions, the type of trajectory followed and the sampling time affect the system state constructibility. Our next steps will move toward using this result to define formally correct strategies for motion control that maximise the system observability (i.e., the possibility of reconstructing the system state).

REFERENCES

[1] M. Ridolfi, S. Van de Velde, H. Steendam, and E. De Poorter, "Analysis of the scalability of uwb indoor localization solutions for high user densities," *Sensors*, vol. 18, no. 6, p. 1875, 2018.

[2] A. Gupta and P. Mohapatra, "A survey on ultra wide band medium access control schemes," *Computer Networks*, vol. 51, no. 11, pp. 2976–2993, 2007.

[3] S. Wu, Y. Ma, Q. Zhang, and N. Zhang, "Nlos error mitigation for uwb ranging in dense multipath environments," in *2007 IEEE Wireless Communications and Networking Conference*. IEEE, 2007, pp. 1565–1570.

[4] L. Palopoli and D. Fontanelli, "Global Observability Analysis of a Nonholonomic Robot using Range Sensors," in *Proc. European Control Conference (ECC)*. Saint Petersburg, Russia: IFAC, May 2020, pp. 1300–1305.

[5] D. Fontanelli, F. Shamsfakhr, D. Macii, and L. Palopoli, "An Uncertainty-driven and Observability-based State Estimator for Nonholonomic Robots," *IEEE Trans. on Instrumentation and Measurement*, vol. 70, pp. 1–12, January 2021.

[6] D. Fontanelli, "Perception for Autonomous Systems: A Measurement Perspective on Localisation and Positioning," *IEEE Instrumentation Measurement Magazine*, vol. 25, no. 4, pp. 4–9, June 2022.

[7] F. M. Ham and R. G. Brown, "Observability, eigenvalues, and kalman filtering," *IEEE Transactions on Aerospace and Electronic Systems*, no. 2, pp. 269–273, 1983.

[8] J. F. Grcar, "Optimal sensitivity analysis of linear least squares," *Lawrence Berkeley National Laboratory, Report LBNL-52434*, vol. 99, 2003.

[9] F. Shamsfakhr, D. Macii, D. Fontanelli, L. Palopoli, A. Motroni, P. Nepa, and A. Buffi, "RFID-based robot localisation: an unconstrained optimisation problem by exploiting RSSI," in *Proc. IEEE Int. Instrumentation and Measurement Technology Conference (I2MTC)*. Ottawa, Canada: IEEE, May 2022, to appear.